Mechanism and Machine Theory 70 (2013) 278–292

Contents lists available at ScienceDirect

Mechanism and Machine Theory

journal homepage: www.elsevier.com/locate/mechmt

A 6*R* linkage reconfigurable between the line-symmetric Bricard linkage and the Bennett linkage

C.Y. Song [a], Yan Chen [b,*], I-Ming Chen [a]

[a] School of Mechanical and Aerospace Engineering, Nanyang Technological University, 50 Nanyang Avenue, Singapore 639798, Singapore
[b] Key Laboratory of Mechanism Theory and Equipment Design of Ministry of Education, Tianjin University, Tianjin 300072, China

ARTICLE INFO

Article history:
Received 26 May 2013
Received in revised form 15 July 2013
Accepted 17 July 2013
Available online 22 August 2013

Keywords:
Line-symmetric Bricard linkage
Bennett linkage
Spatial triangle
Reconfigurable mechanism
Bifurcation analysis

ABSTRACT

This paper explores the feasibility of constructing mechanisms reconfigurable between 6*R* and 4*R* overconstrained linkages. Spatial triangle and Bennett linkage are used as the building blocks to form the reconfigurable Bricard linkage. Due to the different directions of the joint axes, the Bennett linkage can be setup in either asymmetric or line-symmetric manners. Subsequently, two 6*R* linkages are constructed in asymmetric and line-symmetric configurations, respectively. Their potential of reconfiguration is investigated through bifurcation analysis. The result shows that the asymmetric one can be reconfigured between Bennett linkage and general line-symmetric Bricard linkage through bifurcation points, while the line-symmetric one only functions as a Bennett linkage with two additional fixed joints.

1. Introduction

There are two major linkage families among the various single-loop overconstrained spatial linkages: the Bennett-based one [1] and the Bricard-related one. In the former one, the Bennett linkage [2,3] is used as the basic construct unit to form different overconstrained 5*R* and 6*R* linkages, such as Myard linkages [4], extended Myard linkage [5], Goldberg's 5*R* and 6*R* linkages [6], Waldron's hybrid 6*R* linkages [7], Yu and Baker's syncopated 6*R* linkage [8], generalised Goldberg 5*R* linkage and Wohlhart's double-Goldberg 6*R* linkage [9], mixed double-Goldberg 6*R* linkages [10] and so on. Linkages in the Bricard-related family usually contain certain symmetric geometry properties to enable mobility [11,12], including three octahedral cases [13], three linkage cases [14], Altmann's 6*R* linkage [15], Wohlhart's hybrid 6*R* linkage [16] and so on. However, there is little interaction between the linkages in Bennett-based linkage family and those in Bricard-related one, except for the isomerization introduced by Wohlhart [17], which sets up the connection between the Wohlhart's double-Goldberg 6*R* linkage and the line-symmetric Bricard linkage.

Recent development in mechanism and machine design promotes the concept of reconfigurable mechanism, which has emerged into three major categories. The first is based on the re-assembly of identical or similar robotics modules [18–20], each of which is an integrated system of microprocessors, batteries, sensors, end-effectors, etc. The second is the metamorphic mechanism [21–23], which can generate different topologies for reconfigurations. The third is to incorporate certain bifurcation behaviours to the existing linkage's kinematic paths [24–26]. At the transit configurations, kinematotropy mechanism [25,27] can change its global mobility. The mechanism reported by Kong and Huang [24] can change between two operation modes. And the multifunctional 7*R* mechanism can function as two different types of overconstrained linkages [26]. A comprehensive review about the current development, principles and strategies of the reconfigurable mechanisms was discussed in [28]. The potential of reconfiguration can be identified when two or more subgroups are involved in the construct of the mechanism [29]. The

* Corresponding author. Tel.: +86 22 27406136.
E-mail address: yan_chen@tju.edu.cn (Y. Chen).

0094-114X/$ – see front matter © 2013 Elsevier Ltd. All rights reserved.
http://dx.doi.org/10.1016/j.mechmachtheory.2013.07.013

Section 0, i.e. 0. Notation

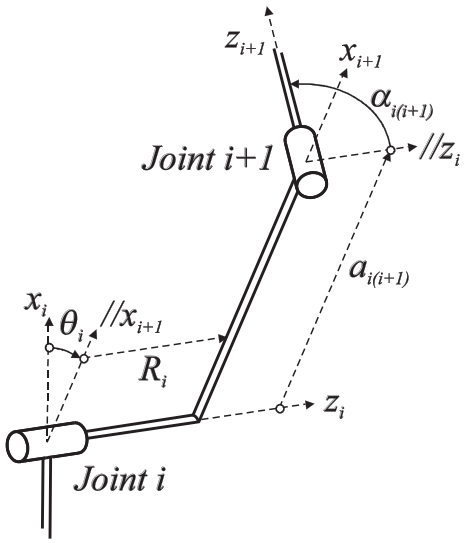

Fig. 0. The setup of the Denavit and Hartenberg's parameters.

z_i The coordinate axis along the revolute axis of joints i;

x_i The coordinate axis along the common normal between joint axes z_{i-1} and z_i;

$a_{i(i+1)}$ The length of link $i(i+1)$, which is the common normal distance from z_i to z_{i+1} positively about x_{i+1}, and defined in the range of $(-\infty, +\infty)$;

$a_{i(i+1)}$ The twist of link $i(i+1)$, which is the rotation angle from z_i to z_{i+1} positively about x_{i+1}, and defined in the range of $[-\pi, \pi)$;

R_i The offset of joint i, which is the common normal distance from x_i to x_{i+1} positively along z_i, and defined in the range of $(-\infty, +\infty)$;

θ_i The revolute variable of joint i, which is the rotation angle from x_i to x_{i+1} positively about z_i, and defined in the range of $[-\pi, \pi)$;

$\mathbf{T}_{i(i+1)}$ The transformation matrix from joint i to joint $i+1$;

$$\mathbf{T}_{i(i+1)} = \begin{bmatrix} \cos\theta_i & -\cos\alpha_{i(i+1)}\sin\theta_i & \sin\alpha_{i(i+1)}\sin\theta_i & a_{i(i+1)}\cos\theta_i \\ \sin\theta_i & \cos\alpha_{i(i+1)}\cos\theta_i & -\sin\alpha_{i(i+1)}\cos\theta_i & a_{i(i+1)}\sin\theta_i \\ 0 & \sin\alpha_{i(i+1)} & \cos\alpha_{i(i+1)} & R_i \\ 0 & 0 & 0 & 1 \end{bmatrix};$$

Aterm, *Bterm*, *Cterm*, *A*, *B*, *C* Simplified mathematical symbols;

$A_{2,3}$, $B_{2,3}$, $C_{2,3}$, $D_{2,3}$, $E_{2,3}$, $F_{2,3}$, $G_{2,3}$, $H_{2,3}$, $L_{2,3}$ Simplified mathematical symbols;

i Denotes joint sequence in the resultant asymmetric Bricard linkage in Section 3;

i' Denotes joint sequence in the resultant line-symmetric Bricard linkage in Section 4;

ST, AB, LB Superscripts that denote parameters in the spatial triangle (ST), Bennett linkage in asymmetric setup (AB) and Bennett linkage in line-symmetric setup (LB); and

$B_{I,II}$ Bifurcation points on the kinematic paths.

bifurcation behaviour of the double-subtractive-Goldberg 6*R* linkage was analysed in [30], where multiple linkage closures were found using both construct method and non-construct method. As the result, this Goldberg 6*R* linkage could be reconfigured among four different 6*R* linkages, whose kinematic curves form a closed loop through four bifurcation points. Recently, the Wohlhart's double-Goldberg 6*R* linkage was analysed and the operation form of a 4*R* linkage is successfully introduced to the linkage's bifurcation paths [31]. Here, the effort is made to construct reconfigurable mechanism under the third category.

In this paper, two spatial triangles and Bennett linkages are used as the basic elements to construct the 6*R* linkages with different reconfiguration capabilities. In Section 2, the kinematics of the spatial triangle, the Bennett linkage and the general line-symmetric Bricard linkage are introduced. Sections 3 and 4 demonstrate the construct process of an asymmetric 6*R* linkage and a line-symmetric 6*R* linkage, as well as analyse their kinematic bifurcation for reconfiguration. Final conclusions are drawn in Section 5.

2. Preliminaries

2.1. The spatial triangle structure

The spatial triangle is a single-loop structure enclosed by three spatial links and connected by three revolute joints. It was initially introduced and analysed by Yang [32] using dual quaternion method. Later, Mavroidis and Roth [33] studied the kinematics of the spatial polygons using matrix method and extended the research into screw polygons. And screw triangles were applied to unify the finite and infinitesimal kinematics [34]. The importance of spatial triangle was recently revisited by Huang [35]. In Fig. 1, a spatial triangle is defined with DH parameters [36].

With the geometry conditions of links 12 and 23 in the spatial triangle, i.e. a_{12}, α_{12}, a_{23}, α_{23}, R_2 and θ_2, using the closure matrix condition that

$$\mathbf{T}_{12}\mathbf{T}_{23}\mathbf{T}_{31} = \mathbf{I}, \tag{1}$$

the geometric parameters on link 31 can be derived as

$$\begin{aligned}
a_{31} &= a_{23}(\cos\alpha_{12}\sin\theta_1\sin\theta_2 - \cos\theta_1\cos\theta_2) - a_{12}\cos\theta_1 - R_2\sin\alpha_{12}\sin\theta_1,\\
\tan\alpha_{31} &= -\frac{\sin\alpha_{12}\sin\theta_2}{\sin\theta_1\cos\theta_2 + \cos\alpha_{12}\sin\theta_2\cos\theta_1},\\
R_1 &= \frac{a_{12}(\cos\alpha_{31}\sin\theta_1\sin\theta_3 - \cos\theta_1\cos\theta_3) - a_{23} - a_{31}\cos\theta_3}{\sin\alpha_{31}\sin\theta_3},\\
R_3 &= \frac{a_{31}(\cos\alpha_{23}\sin\theta_2\sin\theta_3 - \cos\theta_2\cos\theta_3) - a_{12} - a_{23}\cos\theta_2}{\sin\alpha_{31}\sin\theta_3},\\
\tan\theta_1 &= -\frac{\sin\alpha_{23}\sin\theta_2}{\sin\alpha_{12}\cos\alpha_{23} + \cos\alpha_{12}\sin\alpha_{23}\cos\theta_2},\\
\tan\theta_3 &= -\frac{\sin\alpha_{12}\sin\theta_2}{\sin\alpha_{23}\cos\alpha_{12} + \cos\alpha_{23}\sin\alpha_{12}\cos\theta_2}.
\end{aligned} \tag{2}$$

2.2. The Bennett linkage with two different setups

The original setup of the Bennett linkage [2,3] is shown in Fig. 2(a). Its geometry conditions and closure equations are

$$a_{12} = a_{34}, \alpha_{12} = \alpha_{34}, a_{23} = a_{41}, \alpha_{23} = \alpha_{41}, R_i = 0 (i = 1,\ 2,\ 3 \text{ and } 4), \tag{3a}$$

$$\frac{\sin\alpha_{12}}{a_{12}} = \frac{\sin\alpha_{23}}{a_{23}}; \tag{3b}$$

and

$$\theta_1 + \theta_3 = 0, \tag{4a}$$

$$\theta_2 + \theta_4 = 0, \tag{4b}$$

$$\tan\frac{\theta_1}{2}\tan\frac{\theta_2}{2} = \frac{\sin\frac{\alpha_{23}+\alpha_{12}}{2}}{\sin\frac{\alpha_{23}-\alpha_{12}}{2}}, \tag{4c}$$

respectively.

The proportional relationship of the sine of twist over link length is called the *Bennett ratio*, as shown in Eq. (3b). The geometry conditions in Eqs. (3a) and (3b) are typically in a line-symmetric form. But the closure equations in Eqs. (4a) and (4b) do not follow the line-symmetric condition. This is because the revolute axes of the Bennett linkage in Fig. 2(a) are not set up in a

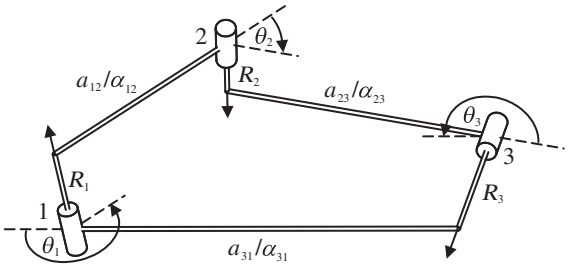

Fig. 1. A spatial triangle defined with DH parameters.

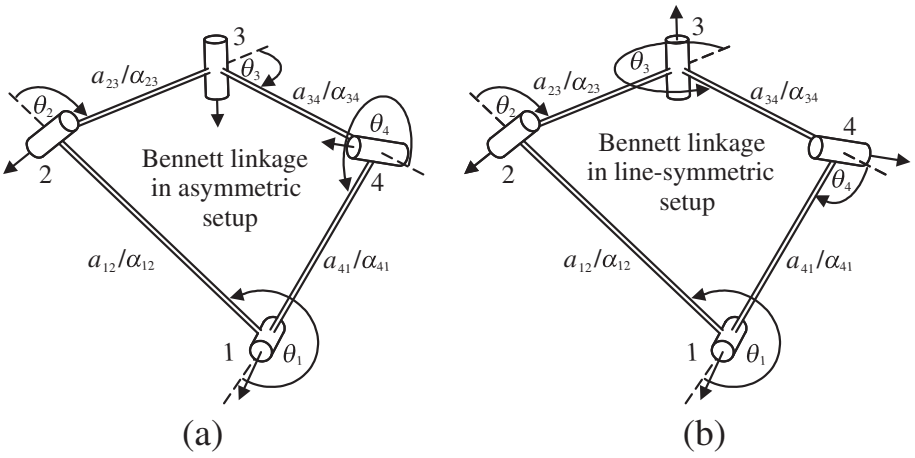

Fig. 2. The two different joint-axis setups of Bennett linkage: (a) in the asymmetric setup; (b) in the line-symmetric setup.

line-symmetric manner. As shown in Fig. 2(b), by reversing the axes of joints 3 and 4, the resultant linkage becomes a Bennett linkage in a line-symmetric setup [37,38]. The corresponding geometry conditions and closure equations are

$$a_{12} = a_{34}, \alpha_{12} = \alpha_{34}, a_{23} = a_{41}, \alpha_{23} = \alpha_{41}, R_i = 0 (i = 1,\ 2,\ 3 \text{ and } 4), \tag{5a}$$

$$\frac{\sin\alpha_{12}}{a_{12}} = -\frac{\sin\alpha_{23}}{a_{23}}; \tag{5b}$$

and

$$\theta_1 = \theta_3, \theta_2 = \theta_4, \tan\frac{\theta_1}{2}\tan\frac{\theta_2}{2} = \frac{\cos\frac{\alpha_{23}+\alpha_{12}}{2}}{\cos\frac{\alpha_{23}-\alpha_{12}}{2}}, \tag{6}$$

respectively.

2.3. The general line-symmetric Bricard linkage

The geometry conditions of the general line-symmetric Bricard linkage [14,39] are

$$\begin{aligned} &a_{12} = a_{45},\ a_{23} = a_{56},\ a_{34} = a_{61},\\ &\alpha_{12} = \alpha_{45},\ \alpha_{23} = \alpha_{56},\ \alpha_{34} = \alpha_{61},\\ &R_1 = R_4,\ R_2 = R_5,\ R_3 = R_6. \end{aligned} \tag{7}$$

The explicit closure equations of the linkage have been derived in [40] and two closures of general line-symmetric Bricard linkage forms are found with the identical geometry conditions, whose explicit closure equations are

$$\begin{cases} \theta_2 = 2\tan^{-1}\left(\dfrac{-Bterm_2 + \sqrt{Bterm_2^2 - 4Aterm_2 \cdot Cterm_2}}{2Aterm_2}\right)\\ \theta_3 = 2\tan^{-1}\left(\dfrac{-Bterm_3 - \sqrt{Bterm_3^2 - 4Aterm_3 \cdot Cterm_3}}{2Aterm_3}\right).\\ \theta_4 = \theta_1\\ \theta_5 = \theta_2\\ \theta_6 = \theta_3 \end{cases} \tag{8}$$

And

$$\begin{cases} \theta_2 = 2\tan^{-1}\left(\dfrac{-Bterm_2 - \sqrt{Bterm_2^2 - 4Aterm_2 \cdot Cterm_2}}{2Aterm_2}\right) \\ \theta_3 = 2\tan^{-1}\left(\dfrac{-Bterm_3 + \sqrt{Bterm_3^2 - 4Aterm_3 \cdot Cterm_3}}{2Aterm_3}\right) \\ \theta_4 = \theta_1 \\ \theta_5 = \theta_2 \\ \theta_6 = \theta_3 \end{cases}, \tag{9}$$

respectively. All symbols are defined as follows.

$$\begin{cases} Aterm_2 = (A_2 \sin\theta_1 + B_2 \cos\theta_1 + L_2) - (D_2 + F_2 \sin\theta_1 + H_2 \cos\theta_1) \\ Bterm_2 = 2(C_2 + E_2 \sin\theta_1 + G_2 \cos\theta_1) \\ Cterm_2 = (A_2 \sin\theta_1 + B_2 \cos\theta_1 + L_2) + (D_2 + F_2 \sin\theta_1 + H_2 \cos\theta_1), \end{cases} \tag{10}$$

$$\begin{cases} Aterm_3 = (A_3 \sin\theta_1 + B_3 \cos\theta_1 + L_3) - (D_3 + F_3 \sin\theta_1 + H_3 \cos\theta_1) \\ Bterm_3 = 2(C_3 + E_3 \sin\theta_1 + G_3 \cos\theta_1) \\ Cterm_3 = (A_3 \sin\theta_1 + B_3 \cos\theta_1 + L_3) + (D_3 + F_3 \sin\theta_1 + H_3 \cos\theta_1), \end{cases} \tag{11}$$

$$\begin{cases} A_2 = +(a_{34} \sin\alpha_{12} \cos\alpha_{23} + a_{12} \sin\alpha_{34}) \\ B_2 = -(R_3 \sin\alpha_{12} \cos\alpha_{23} \sin\alpha_{34} + R_2 \sin\alpha_{12} \sin\alpha_{34}) \\ C_2 = +(a_{23} \sin\alpha_{12} \cos\alpha_{34} + a_{12} \sin\alpha_{23}) \\ D_2 = -(R_3 \sin\alpha_{12} \sin\alpha_{23} \cos\alpha_{34} + R_1 \sin\alpha_{12} \sin\alpha_{23}) \\ E_2 = +R_3 \sin\alpha_{23} \sin\alpha_{34} \\ F_2 = +(a_{34} \cos\alpha_{12} \sin\alpha_{23} + a_{23} \sin\alpha_{34}) \\ G_2 = +(a_{23} \cos\alpha_{12} \sin\alpha_{34} + a_{34} \sin\alpha_{23}) \\ H_2 = -R_3 \cos\alpha_{12} \sin\alpha_{23} \sin\alpha_{34} \\ L_2 = +R_1(\cos\alpha_{12} \cos\alpha_{23} + \cos\alpha_{34}) + R_2(\cos\alpha_{23} + \cos\alpha_{12} \cos\alpha_{34}) \\ \quad + R_3(1 + \cos\alpha_{12} \cos\alpha_{23} \cos\alpha_{34}), \end{cases} \tag{12}$$

$$\begin{cases} A_3 = +(a_{12} \cos\alpha_{23} \sin\alpha_{34} + a_{34} \sin\alpha_{12}) \\ B_3 = -(R_2 \sin\alpha_{12} \cos\alpha_{23} \sin\alpha_{34} + R_3 \sin\alpha_{12} \sin\alpha_{34}) \\ C_3 = +(a_{23} \cos\alpha_{12} \sin\alpha_{34} + a_{34} \sin\alpha_{23}) \\ D_3 = -(R_2 \cos\alpha_{12} \sin\alpha_{23} \sin\alpha_{34} + R_1 \sin\alpha_{23} \sin\alpha_{34}) \\ E_3 = +R_2 \sin\alpha_{12} \sin\alpha_{23} \\ F_3 = +(a_{12} \sin\alpha_{23} \cos\alpha_{34} + a_{23} \sin\alpha_{12}) \\ G_3 = +(a_{23} \sin\alpha_{12} \cos\alpha_{34} + a_{12} \sin\alpha_{23}) \\ H_3 = -R_2 \sin\alpha_{12} \sin\alpha_{23} \cos\alpha_{34} \\ L_3 = +R_1(\cos\alpha_{12} + \cos\alpha_{23} \cos\alpha_{34}) + R_2(1 + \cos\alpha_{12} \cos\alpha_{23} \cos\alpha_{34}) \\ \quad + R_3(\cos\alpha_{23} + \cos\alpha_{12} \cos\alpha_{34}). \end{cases} \tag{13}$$

3. The asymmetric 6*R* linkage

Two identical spatial triangles 123 and 456 are prepared for construction in Fig. 3, whose geometry conditions are set up as follows.

$$\begin{array}{llll} a_{45}^{ST} = a_{12}^{ST}, & \alpha_{45}^{ST} = \alpha_{12}^{ST}, & R_4^{ST} = R_1^{ST}, & \theta_4^{ST} = \theta_1^{ST}, \\ a_{56}^{ST} = a_{23}^{ST}, & \alpha_{56}^{ST} = \alpha_{23}^{ST}, & R_5^{ST} = R_2^{ST}, & \theta_5^{ST} = \theta_2^{ST}, \\ a_{64}^{ST} = a_{31}^{ST}, & \alpha_{64}^{ST} = \alpha_{31}^{ST}, & R_6^{ST} = R_3^{ST}, & \theta_6^{ST} = \theta_3^{ST}. \end{array} \tag{14}$$

Take spatial triangle 123 for example, the geometry conditions on links 12 and 23, i.e. a_{12}^{ST}, α_{12}^{ST}, a_{23}^{ST}, α_{23}^{ST}, θ_2^{ST} and R_2^{ST} are *pre-defined* design parameters. The rest of the parameters related to link 31 can be derived with Eq. (2).

Bennett linkage 1346 in asymmetric joint-axis setup, as the original Bennett linkage, is used as an intermediate bridge to connect these two spatial triangles. Bennett linkage 1346 and spatial triangle 123 share the common link 31 for merging. Note that the joint axes on the links to be merged should be kept along the same directions. This is the same for merging Bennett linkage 1346 and spatial triangle 456 on link 46. Therefore, the geometry conditions of the Bennett linkage 1346 in asymmetric

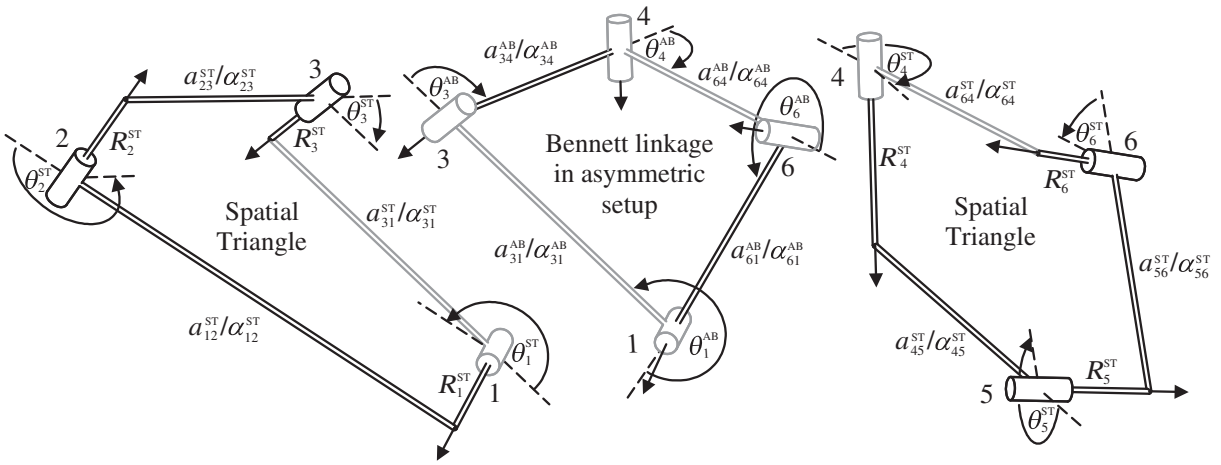

Fig. 3. The construct of the asymmetric 6*R* linkage.

setup are

$$\begin{aligned} a_{31}^{AB} = a_{64}^{AB} = a_{31}^{ST}\left(= a_{64}^{ST}\right),\ a_{34}^{AB} = a_{61}^{AB},\\ \alpha_{31}^{AB} = \alpha_{64}^{AB} = \alpha_{31}^{ST}\left(= \alpha_{64}^{ST}\right),\ \alpha_{34}^{AB} = \alpha_{61}^{AB},\\ \frac{\sin\alpha_{31}^{AB}}{a_{31}^{AB}} = \frac{\sin\alpha_{34}^{AB}}{a_{34}^{AB}}, R_i^{AB} = 0 (i = 1,\ 3,\ 4 \text{ and } 6). \end{aligned} \tag{15}$$

In Fig. 4, after removing the common links and joints marked in dash lines, the rest form a single-loop overconstrained 6*R* linkage. Its geometry conditions are directly related to those of the spatial triangle and Bennett linkage as

$$a_{12} = a_{45} = a_{12}^{ST},\ a_{23} = a_{56} = a_{23}^{ST},\ a_{34} = a_{61} = a_{34}^{AB}, \tag{16a}$$

$$\alpha_{12} = \alpha_{45} = \alpha_{12}^{ST},\ \alpha_{23} = \alpha_{56} = \alpha_{23}^{ST},\ \alpha_{34} = \alpha_{61} = \alpha_{34}^{AB}, \tag{16b}$$

$$\frac{\sin\alpha_{34}}{\alpha_{34}} = \frac{\sin\alpha_{31}^{ST}}{\alpha_{31}^{ST}}, \tag{16c}$$

$$R_1 = R_4 = R_1^{ST},\ R_2 = R_5 = R_2^{ST},\ R_3 = R_6 = R_3^{ST}. \tag{16d}$$

Thus, this 6*R* linkage belongs to the general line-symmetric Bricard linkage with $\theta_{2,5}$ fixed at θ_2^{ST}.

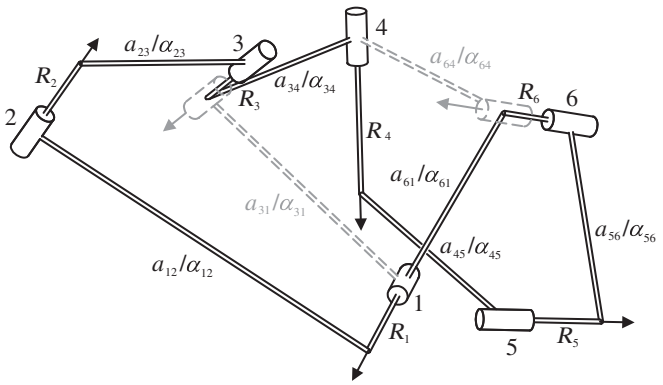

Fig. 4. The first reconfigurable asymmetric 6*R* linkage.

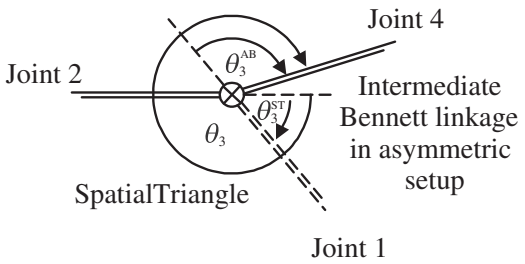

Fig. 5. The compatibility condition of joint 3 in the first reconfigurable 6*R* linkage.

The explicit closure equations of this 6*R* linkage could be derived by analysing the detailed relationship among θ_i, θ_i^{ST} and θ_i^{AB}. For example, the construct process of joint 3 in Fig. 5 determines

$$\theta_3 = \theta_3^{ST} + \theta_3^{AB} + \pi. \tag{17}$$

As a result, the compatibility conditions for the asymmetric 6*R* linkage are

$$\begin{aligned} &\theta_1 = \theta_1^{ST} + \theta_1^{AB} - \pi,\ \ \theta_2 = \theta_2^{ST},\ \ \theta_3 = \theta_3^{ST} + \theta_3^{AB} + \pi, \\ &\theta_4 = \theta_1^{ST} - \theta_1^{AB} - \pi,\ \ \theta_5 = \theta_2^{ST},\ \ \theta_6 = \theta_3^{ST} - \theta_3^{AB} - \pi. \end{aligned} \tag{18}$$

By substituting the closure equations of the spatial triangle in Eq. (2) and that of the asymmetric Bennett linkage in Eqs. (4a)–(4c) into Eq. (18), we can derive the explicit closure equations of this linkage as follows.

$$\begin{aligned} &\theta_1 + \theta_4 = 2\theta_1^{ST},\ \ \theta_2 = \theta_5 = \theta_2^{ST},\ \ \theta_3 + \theta_6 = 2\theta_3^{ST}, \\ &\theta_3 = \theta_3^{ST} - 2\tan^{-1}\left(\frac{\sin\frac{\alpha_{34} + \alpha_{31}^{ST}}{2}}{\sin\frac{\alpha_{34} - \alpha_{31}^{ST}}{2}} \cdot \tan\frac{\theta_1 - \theta_1^{ST}}{2}\right) + \pi, \end{aligned} \tag{19}$$

where $\theta_{1,3}^{ST}$ and α_{31}^{ST} are determined in Eq. (2) with *pre-defined* design parameters $\alpha_{12,23}^{ST}$, $a_{12,23}^{ST}$ and θ_2^{ST}. The kinematic paths are plotted in Fig. 6 using Eq. (19). Note that $\theta_{2,5}$ is constrained to a fixed design parameter of θ_2^{ST} during the full circle movement, which corresponds to the pre-defined configurations of joints 2 and 5 in the spatial triangles. Although the geometry conditions

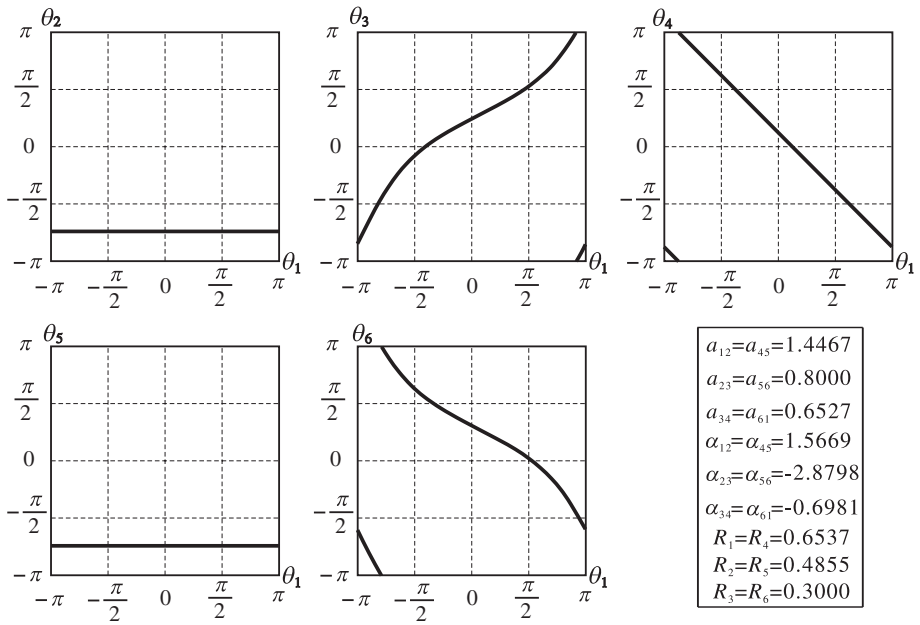

Fig. 6. The kinematic paths of the asymmetric 6*R* linkage.

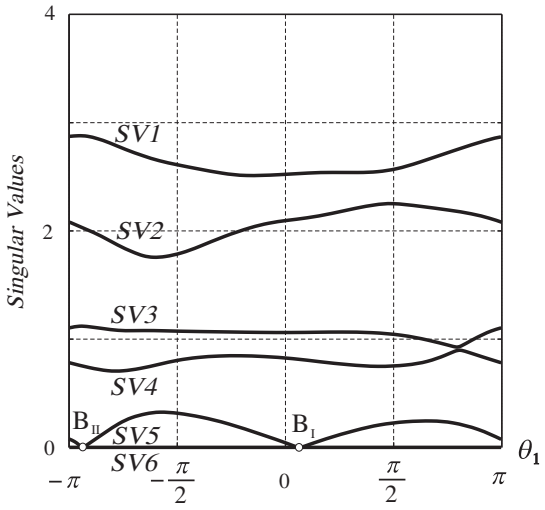

Fig. 7. The SVD results of the asymmetric 6*R* linkage.

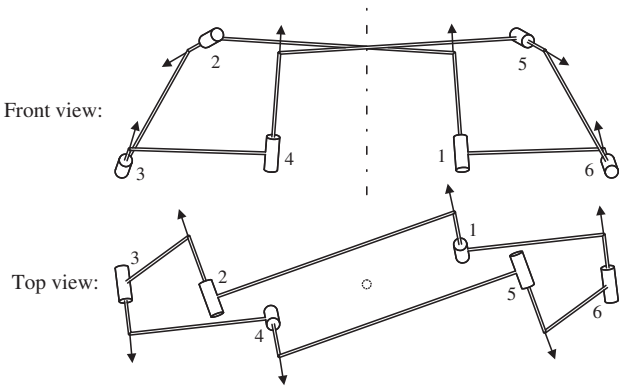

Fig. 8. The configuration of the Form I of the asymmetric 6*R* linkage when $\theta_1 = 14.9739\pi / 180$ and $\theta_2 = (\theta_2^{ST} =) - 70.0000\pi / 180$.

of the 6*R* linkage are line-symmetric in Eqs. (16a)–(16d), the resultant linkage is still kinematically asymmetric with $\theta_1 \neq \theta_4$, $\theta_2 = \theta_5$ and $\theta_3 \neq \theta_6$ in Eq. (19), which is an inherited property from the Bennett linkage in asymmetric setup.

The linkage's singular values are plotted in Fig. 7 using the Singular Value Decomposition method [41,42], in which the fifth singular value falls to zero at B_I and B_{II}, indicating possible bifurcation behaviours. At point B_I, it is found that the linkage could bifurcate into an operation form with six active revolute joints, with line-symmetric property, see Fig. 8. The line of symmetry is shown as the central line in front view and the dashed dot in top view.

By using the SVD method, this linkage's kinematic paths are shown in Fig. 9 and the singular values in Fig. 10. It is found that the kinematic paths are in correspondence to the closure equations in Eq. (8), which indicates that this linkage is a Form I general line-symmetric Bricard linkage. To differentiate the linkages, we name the linkage in Fig. 4 as *the Bennett linkage form*, and the

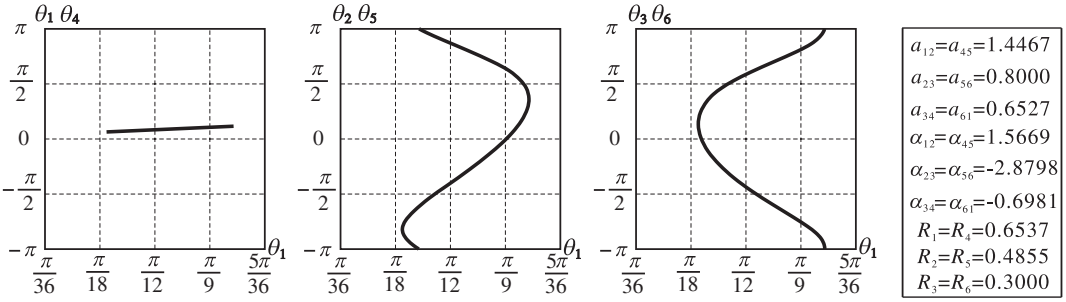

Fig. 9. The kinematic paths of the Form I of the asymmetric 6*R* linkage. Note that the figures are plotted in the region that $\theta_1 \in [\pi / 36, 5\pi / 36]$.

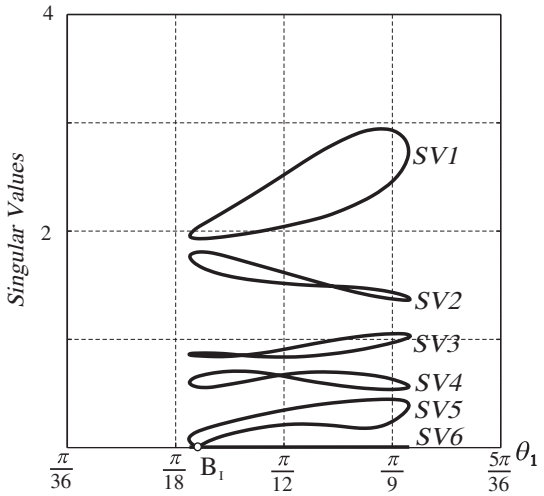

Fig. 10. The SVD results of the Form I of the asymmetric 6*R* linkage.

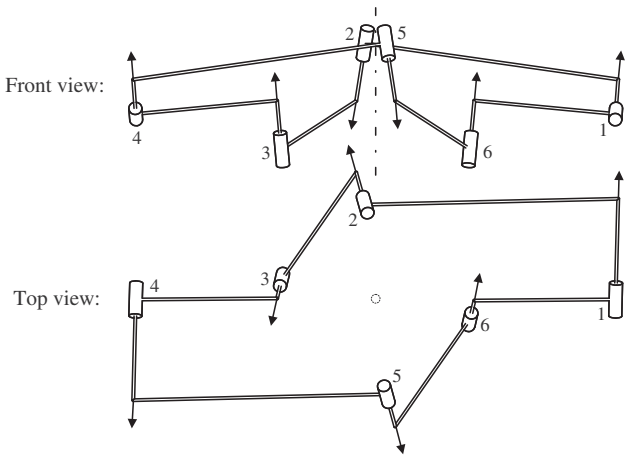

Fig. 11. The configuration of the Form II of the asymmetric 6*R* linkage when $\theta_1 = 176.7291\pi / 180$ and $\theta_2 = (\theta_2^{ST} =) - 70.0000\pi / 180$.

linkage in Fig. 8 as *the Form I linkage*. In Fig. 10, the fifth singular value falls to zero at B_I, which is in accordance to the SVD results in Fig. 7. The location of $\theta_1^{B_I}$ can be determined analytically in Eq. (20) by substituting the *pre-defined* revolute parameter θ_2^{ST} on joint 2 in the Bennett linkage form into the closure equations of the Form I general line-symmetric Bricard linkage in Eq. (8). The solution to Eq. (20) is derived in Appendix A.

$$\tan\frac{\theta_2^{ST}}{2} = \frac{-Bterm_2 + \sqrt{Bterm_2^2 - 4Aterm_2 \cdot Cterm_2}}{2Aterm_2} \tag{20}$$

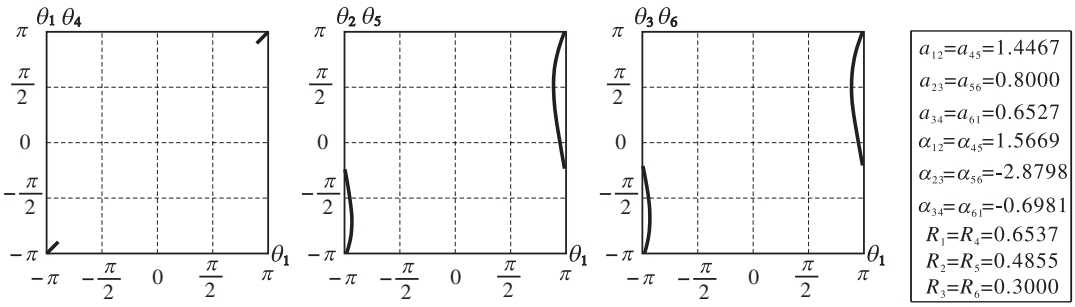

Fig. 12. The kinematic paths of the Form II of the asymmetric 6*R* linkage.

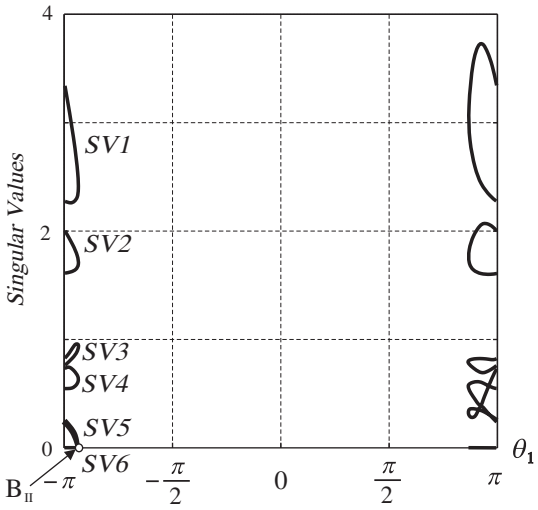

Fig. 13. The SVD results of the Form II of the asymmetric 6*R* linkage.

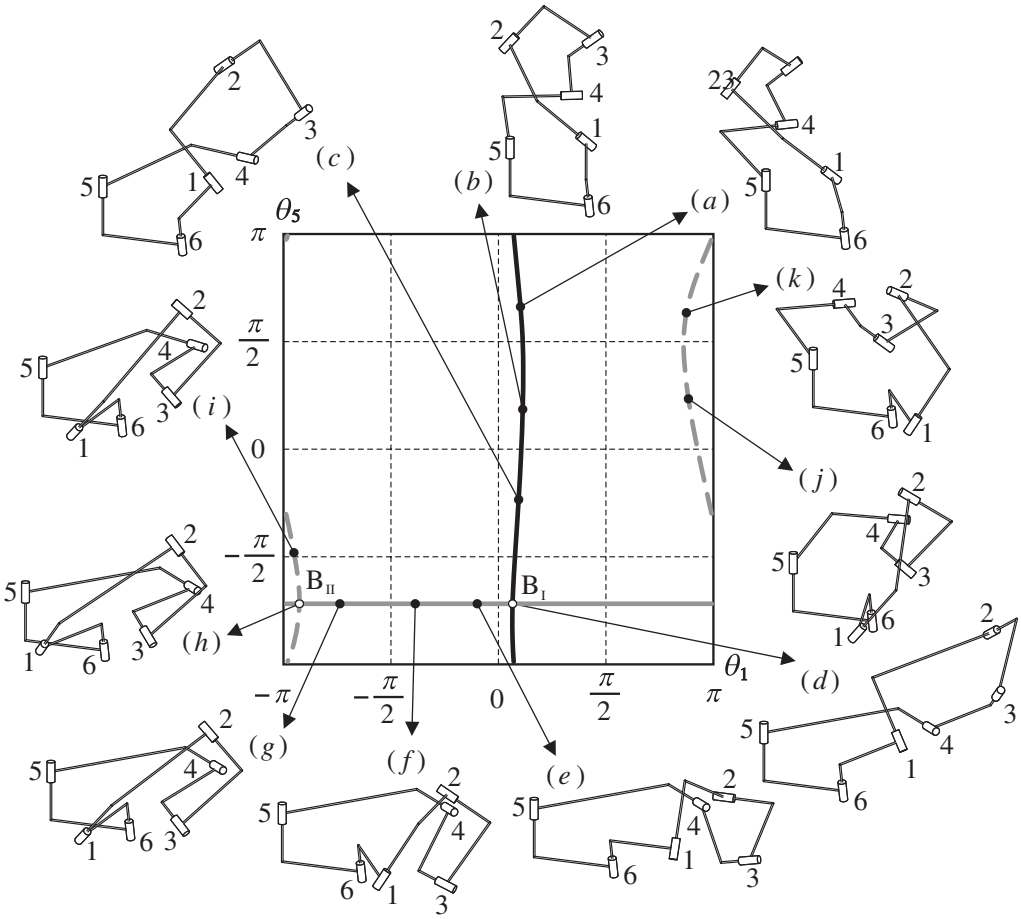

Fig. 14. The transitions of the asymmetric 6*R* linkage with multiple operation forms. (a)–(c) are the motion sequence of the Form I linkage; (d) is the bifurcation configuration between Form I linkage and the Bennett linkage form; (e)–(g) are the motion sequence of the Bennett linkage form; (h) is the bifurcation configuration between the Bennett linkage form and the Form II linkage; (i)–(k) are the motion sequence of the Form II linkage.

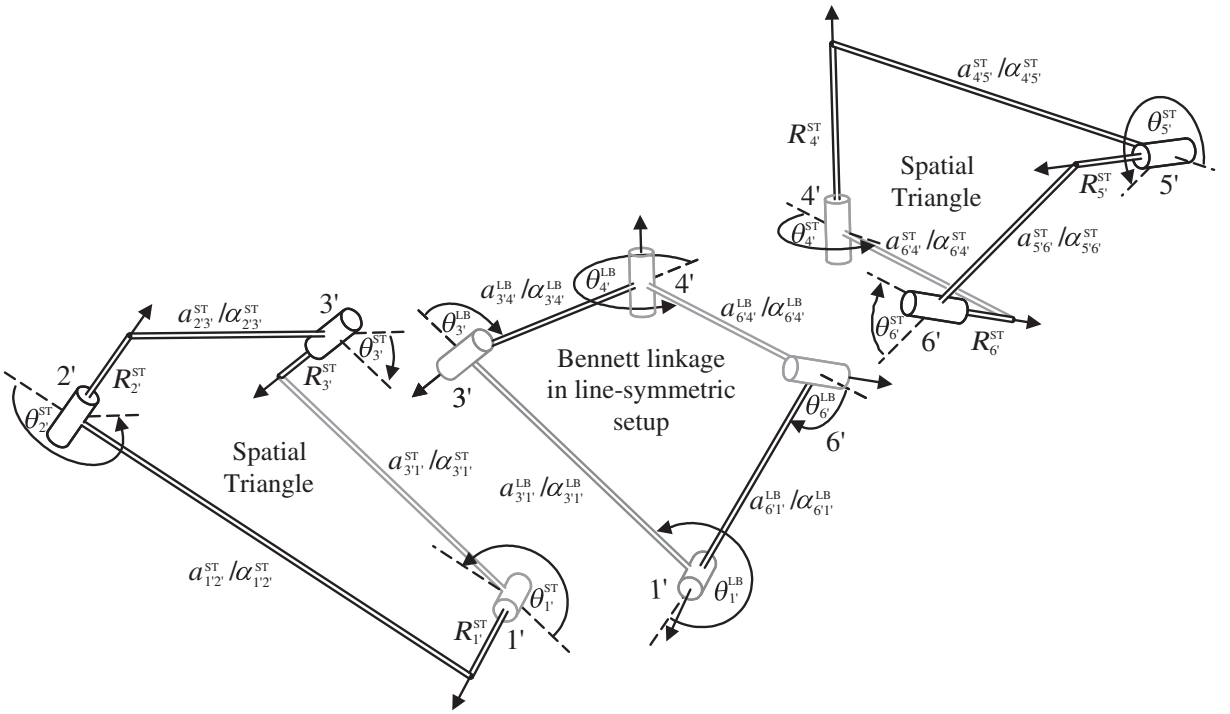

Fig. 15. The construct of the line-symmetric 6*R* linkage.

On the other hand, the Bennett linkage form could bifurcate at B_{II} in Fig. 7 into another operation form with six active revolute joints, see Fig. 11, whose kinematic paths are plotted in Fig. 12 and SVD results in Fig. 13. This linkage's kinematic paths are in correspondence to the closure equations of the Form II general line-symmetric Bricard linkage in Eq. (9) and therefore named as *the Form II linkage*. From the SVD results in Fig. 13, the fifth singular value falls to zero at B_{II}, which is in accordance to the SVD results in Fig. 7. The position of $\theta_1^{B_{II}}$ can be analytically determined in Eq. (21) by substituting the *pre-defined* revolute parameter θ_2^{ST} on joint 2 in the Bennett linkage form into the closure equations of the Form II general line-symmetric Bricard linkage in Eq. (9), whose solution is also included in the Appendix A.

$$\tan\frac{\theta_2^{ST}}{2}=\frac{-Bterm_2-\sqrt{Bterm_2^2-4Aterm_2\cdot Cterm_2}}{2Aterm_2} \tag{21}$$

The full map of bifurcation for the constructed 6*R* linkage is plotted in Fig. 14. The Bennett linkage form can bifurcate into the Form I or Form II linkages on different bifurcation points, but the Form I and II linkages cannot bifurcate into each other directly. Therefore, we successfully introduce the operation form of a Bennett linkage with only 4 active revolute joints to bridge the two forms of the general line-symmetric Bricard linkage. The use of Bennett linkage in asymmetric joint-axis setup disrupts the line-symmetric relationship among the kinematic variables and enables the reconfiguration capability.

4. The line-symmetric 6*R* linkage

As illustrated in Fig. 15, two identical spatial triangles are the same as those in Fig. 3, and the intermediate bridge is a Bennett linkage in line-symmetric joint-axis setup, whose geometry conditions are

$$\begin{gathered}a_{3'1'}^{LB}=a_{6'4'}^{LB}=a_{31}^{AB},\ a_{3'4'}^{LB}=a_{6'1'}^{LB}=a_{34}^{AB},\\ \alpha_{3'1'}^{LB}=\alpha_{6'4'}^{LB}=\alpha_{31}^{AB},\ \alpha_{3'4'}^{LB}=\alpha_{6'1'}^{LB}=\alpha_{34}^{AB}\pm\pi,\\ \frac{\sin\alpha_{3'1'}^{LB}}{a_{3'1'}^{LB}}=-\frac{\sin\alpha_{3'4'}^{LB}}{a_{3'4'}^{LB}},\ R_i^{LB}=0(i=1',\ 3',\ 4'\ \text{and}\ 6').\end{gathered} \tag{22}$$

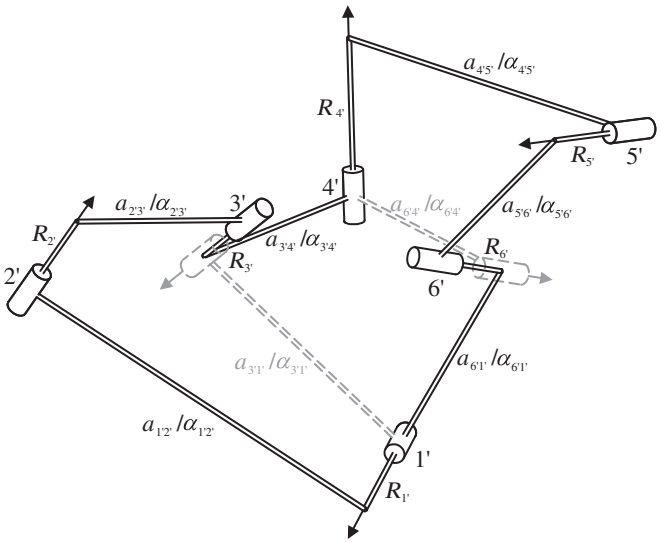

Fig. 16. The line-symmetric 6*R* linkage.

In Fig. 16, after removing the common links and joints in dash lines, the rest form the second 6*R* linkage. Its geometry conditions are

$$a_{1'2'} = a_{4'5'} = a^{\mathrm{ST}}_{1'2'},\ \ a_{2'3'} = a_{5'6'} = a^{\mathrm{ST}}_{2'3'},\ \ a_{3'4'} = a_{6'1'} = a^{\mathrm{LB}}_{3'4'}, \tag{23a}$$

$$\alpha_{1'2'} = \alpha_{4'5'} = \alpha^{\mathrm{ST}}_{1'2'},\ \ \alpha_{2'3'} = \alpha_{5'6'} = \alpha^{\mathrm{ST}}_{2'3'},\ \ \alpha_{3'4'} = \alpha_{6'1'} = \alpha^{\mathrm{LB}}_{3'4'} \tag{23b}$$

$$\frac{\sin\alpha_{3'4'}}{a_{3'4'}} = -\frac{\sin\alpha^{\mathrm{ST}}_{3'1'}}{a^{\mathrm{ST}}_{3'1'}}, \tag{23c}$$

$$R_{1'} = R_{4'} = R^{\mathrm{ST}}_{1'},\ \ R_{2'} = R_{5'} = R^{\mathrm{ST}}_{2'},\ \ R_{3'} = R_{6'} = R^{\mathrm{ST}}_{3'}. \tag{23d}$$

which also belong to the general line-symmetric Bricard linkage with $\theta_{2',5'}$ fixed at $\theta^{\mathrm{ST}}_{2'}$. Following the same procedure as the foregoing section, the closure equations of this 6*R* linkage are derived as follows,

$$\begin{aligned} \theta_{1'} &= \theta_{4'},\ \ \theta_{2'} = \theta_{5'} = \theta^{\mathrm{ST}}_{2'}, \\ \theta_{3'} = \theta_{6'} &= \theta^{\mathrm{ST}}_{3'} - 2\tan^{-1}\left(\frac{\cos\dfrac{\alpha_{3'4'}+\alpha^{\mathrm{ST}}_{3'1'}}{2}}{\cos\dfrac{\alpha_{3'4'}-\alpha^{\mathrm{ST}}_{3'1'}}{2}}\cdot\tan\frac{\theta_{1'}-\theta^{\mathrm{ST}}_{1'}}{2}\right)+\pi, \end{aligned} \tag{24}$$

where $\theta^{\mathrm{ST}}_{1',3'}$ and $\alpha^{\mathrm{ST}}_{3',1'}$ are determined in Eq. (2) with *pre-defined* design parameters $\alpha^{\mathrm{ST}}_{1'2',2'3'}$, $a^{\mathrm{ST}}_{1'2',2'3'}$ and $\theta^{\mathrm{ST}}_{2'}$. Both the geometric conditions and the kinematic variables of the second 6*R* linkage are in line symmetry. Its kinematic paths are plotted in Fig. 17 using Eq. (24), in which $\theta_{2',5'}$ are constrained to the design parameter of $\theta^{\mathrm{ST}}_{2'}$ during the full circle movement. Further investigation shows that the kinematic paths in Fig. 17 are in correspondence to the closure equations of the Form II general line-symmetric Bricard linkage in Eq. (9). Therefore, this Bennett form in Fig. 16 is actually the Form II of the general line-symmetric Bricard linkage with two fixed joints. Its singular values are plotted using SVD method in Fig. 18. There is no singular configuration, which is different from the 6*R* linkage in asymmetric setup. The use of Bennett linkage in line-symmetric setup preserved the line-symmetric relationship among the kinematic variables. Thus, the resultant linkage shares the same kinematic property as the general line-symmetric Bricard linkage, which is not reconfigurable [40]. The kinematic paths of the corresponding Form I linkage is shown in Fig. 19 using Eq. (8), which confirms that there is no common configuration between the Forms I and II linkages of the second 6*R* linkage we just constructed.

5. Conclusion

In this paper, the feasibility of reconfiguration between the general line-symmetric Bricard linkage and the Bennett linkage is explored base on their symmetry property. By using spatial triangles and Bennett linkages in different symmetry joint-axis setups as the building blocks, two 6*R* linkages have been constructed.

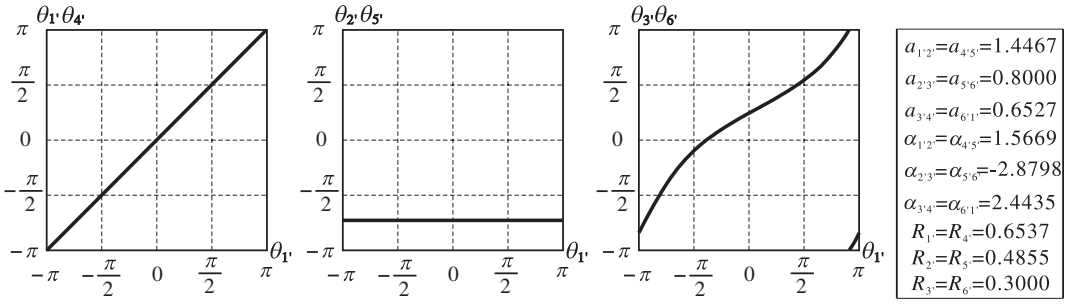

Fig. 17. The kinematic paths of the line-symmetric 6*R* linkage.

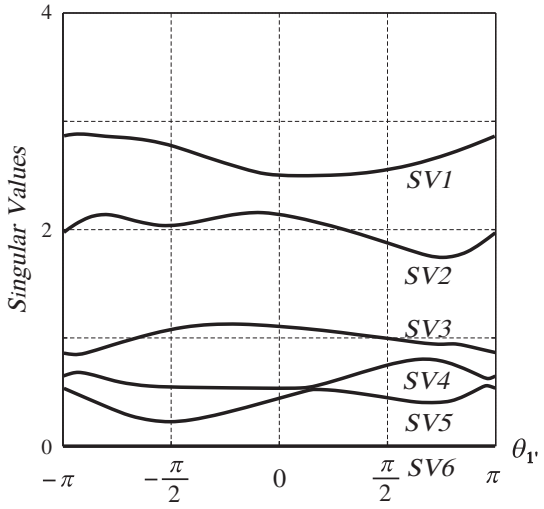

Fig. 18. The SVD results of the line-symmetric 6*R* linkage.

The first 6*R* linkage is achieved by connecting two identical spatial triangles with a Bennett linkage in asymmetric joint-axis setup, and then removing the redundant links inside to form a closed-loop overconstrained spatial linkage. The kinematic singularity analysis reveals that this linkage is actually in a Bennett linkage form and reconfigurable to the Forms I and II line-symmetric Bricard linkage through bifurcation points. Therefore, it is a reconfigurable linkage.

By replacing the Bennett linkage in asymmetric joint-axis setup with a Bennett linkage in line-symmetric setup in the construction, the second 6*R* linkage has been formed. The second linkage shares the same kinematic properties with the general line-symmetric Bricard linkage and it is not reconfigurable between the two linkage forms. The constructed 6*R* linkage is a special case of the Form II line-symmetric Bricard linkage with two fixed joints. A summary of these two linkages is listed in Table 1.

Here, the construct method for the proposed reconfigurable Bricard linkage has been developed. For a given line-symmetric Bricard linkage, either reverse-construct method or SVD method can be applied to testify whether it could be reconfigured into a

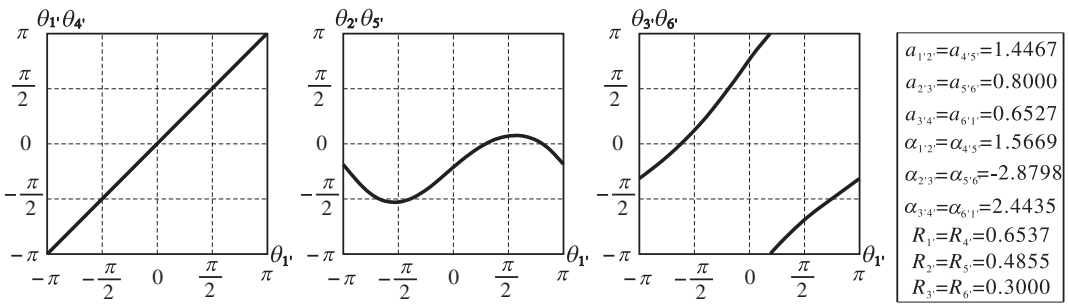

Fig. 19. The kinematic paths of corresponding Form I linkage of the line-symmetric 6*R* linkage.

Table 1
Summary of the two constructed 6*R* linkages.

	The first reconfigurable asymmetric 6*R* linkage	The second line-symmetric 6*R* linkage
Construct units	Two identical spatial triangles & One Bennett linkage in asymmetric joint-axis setup	Two identical spatial triangles & One Bennett linkage in line-symmetric joint-axis setup
Resultant linkage forms	*Bennett linkage form* Form I of the general line-symmetric Bricard linkage Form II of the general line-symmetric Bricard linkage	*Form II of the general line-symmetric Bricard linkage with two fixed joints*
Reconfiguration potential	Reconfigurable through bifurcation points	Not reconfigurable as the resultant linkage forms are still independent and distinct to each other

Bennett linkage. This work not only explores the design method for a reconfigurable mechanism between 4*R* and 6*R* overconstrained linkages, but also sets up a connection between the Bennett linkage and the line-symmetric Bricard linkage.

Acknowledgement

C.-Y. Song would like to thank NTU for providing the University Graduate Scholarship during his PhD study. This work is financially supported by the Natural Science Foundation of China (Projects No. 51275334 and No. 51290293).

Appendix A. The solutions to Eqs. (20) and (21)

The solutions to Eqs. (20) and (21) are derived from the following equations:

$$\tan\frac{\theta_2^{ST}}{2}=\frac{-Bterm_2\pm\sqrt{Bterm_2^2-4Aterm_2\cdot Cterm_2}}{2Aterm_2}. \tag{25}$$

The above equation could be rewritten into the following form,

$$Aterm_2\cdot\tan^2\frac{\theta_2^{ST}}{2}+Bterm_2\cdot\tan\frac{\theta_2^{ST}}{2}+Cterm_2=0, \tag{26}$$

where $Aterm_2$, $Bterm_2$ and $Cterm_2$ are functions of θ_1 in Eqs. (10) and (12). By substituting Eqs. (10) and (12) into Eq. (26), we will get the following equation about $\theta_1^{B_{I/II}}$,

$$A\cdot\sin\theta_1^{B_{I/II}}+B\cdot\cos\theta_1^{B_{I/II}}+C=0, \tag{27}$$

where

$$\begin{cases} A=(A_2-F_2)\tan^2\dfrac{\theta_2^{ST}}{2}+2E_2\tan\dfrac{\theta_2^{ST}}{2}+(A_2-F_2)\\ B=(B_2-H_2)\tan^2\dfrac{\theta_2^{ST}}{2}+2G_2\tan\dfrac{\theta_2^{ST}}{2}+(B_2-H_2)\\ C=(L_2-D_2)\tan^2\dfrac{\theta_2^{ST}}{2}+2C_2\tan\dfrac{\theta_2^{ST}}{2}+(L_2-D_2). \end{cases} \tag{28}$$

After half-tangent transformation of the $\sin\theta_1^{B_{I/II}}$ and $\cos\theta_1^{B_{I/II}}$ in Eq. (28), we can derive that

$$(C-B)\cdot\tan^2\frac{\theta_1^{B_{I/II}}}{2}+2A\cdot\tan\frac{\theta_1^{B_{I/II}}}{2}+(C+B)=0. \tag{29}$$

By solving Eq. (29), we can derive that

$$\tan\frac{\theta_1^{B_{I/II}}}{2}=\frac{-A\pm\sqrt{A^2+B^2-C^2}}{C-B}. \tag{30}$$

Therefore, the positive result of Eq. (30) is the solution to Eq. (20), while the negative result of Eq. (30) is the solution to Eq. (21). The symbols are determined in Eqs. (12) and (28).

References

[1] J.E. Baker, A comparative survey of the Bennett-based, 6-revolute kinematic loops, Mechanism and Machine Theory 28 (1993) 83–96.
[2] G.T. Bennett, A new mechanism, Engineering 76 (1903) 777–778.
[3] G.T. Bennett, The skew isogram mechanism, Proceedings of the London Mathematical Society s2-13 (1914) 151–173.
[4] F.E. Myard, Contribution à la géométrie des systèmes articulés, Bulletin de la Societe Mathematique de France 59 (1931) 183–210.
[5] Y. Chen, Z. You, An extended Myard linkage and its derived 6*R* linkage, Journal of Mechanical Design, Transaction of the ASME 130 (2008) 8.
[6] M. Goldberg, New five-bar and six-bar linkages in three dimensions, Transactions of the ASME 65 (1943) 649–663.
[7] K.J. Waldron, Hybrid overconstrained linkages, Journal of Mechanics 3 (1968) 73–78.
[8] H.C. Yu, J.E. Baker, On the generation of new linkages from Bennett loops, Mechanism and Machine Theory 16 (1981) 473–485.
[9] K. Wohlhart, Merging two general Goldberg 5*R* linkages to obtain a new 6*R* space mechanism, Mechanism and Machine Theory 26 (1991) 659–668.
[10] C.Y. Song, Y. Chen, A family of mixed double-Goldberg 6*R* linkages, Proceedings of the Royal Society of London A 468 (2012) 871–890.
[11] J. Phillips, Freedom in Machinery I: Introducing Screw Theory, Cambridge University Press, Cambridge, 1984.
[12] J. Phillips, Freedom in Machinery II: Screw Theory Exemplified, Cambridge University Press, Cambridge, 1990.
[13] R. Bricard, Mémoire sur la théorie de l'octaèdre articulé, Journal of Pure and Applied Mathematics 3 (1897) 113–150.
[14] R. Bricard, Leçons de cinématique, Gauthier-Villars, Paris, 1927.
[15] P.G. Altmann, Communications to Grodzinski, P. and M'Ewen, E.: link mechanisms in modern kinematics, Proceedings of the Institution of Mechanical Engineers 168 (1954) 877–896.
[16] K. Wohlhart, A new 6R space mechanism, Proceedings of the 7th World Congress on the Theory of Machines and Mechanisms, Sevilla, Spain, 1987, pp. 193–198.
[17] K. Wohlhart, On isomeric overconstrained space mechanisms, Proceedings of the Eights World Congress on the Theory of Machines and Mechanisms, Prague, Czechoslovakia, 1991, pp. 153–158.
[18] I.M. Chen, Theory and Applications of Modular Reconfigurable Robotic Systems, Mechanical Engineering, California Institute of Technology, Pasadena, CA, 1994.
[19] T. Fukuda, T. Ueyama, Cellular Robotics and Micro Robotic Systems, World Scientific, 1994.
[20] M. Yim, Locomotion with a Unit-modular Reconfigurable Robot, Department of Mechanical Engineering, Stanford University, 1994. 157.
[21] J.S. Dai, J. Rees Jones, Mobility in metamorphic mechanisms of foldable/erectable kinds, Journal of Mechanical Design, Transaction of the ASME 121 (1999) 375–382.
[22] L.P. Zhang, J.S. Dai, Reconfiguration of spatial metamorphic mechanisms, Journal of Mechanical Robotics, Transactions of the ASME 1 (2009) 8.
[23] L.P. Zhang, J.S. Dai, An overview of the development on reconfiguration of metamorphic mechanisms, in: M.Z.a.X.K., J.S. Dai (Eds.), Proceedings of the 2009 ASME/IFToMM International Conference on Reconfigurable Mechanisms and Robots, London, UK, 2009, pp. 8–12.
[24] X. Kong, C. Huang, Type synthesis of single-DOF single-loop mechanisms with two operation modes, Proceedings of the 2009 ASME/IFToMM International Conference on Reconfigurable Mechanisms and Robots, London, UK, 2009, pp. 136–141.
[25] K. Wohlhart, Kinematotropic linkages, in: J.L.a.V. Parenti-Castelli (Ed.), The Fifth International Symposium on Advances in Robots Kinematics, Kluwer Academic Publishers, Portoroz, Slovenia, 1996, pp. 359–368.
[26] K. Wohlhart, Multifunctional 7R linkages, Proceedings of the International Symposium on Mechanisms and Machine Theory, AzCIFToMM, Izmir, Turkey, 2010, pp. 85–91.
[27] C. Galletti, P. Fanghella, Single-loop kinematotropic mechanisms, Mechanism and Machine Theory 36 (2001) 743–761.
[28] C.H. Kuo, J.S. Dai, H.S. Yan, Reconfiguration principles and strategies for reconfigurable mechanisms, Proceedings of the 2009 ASME/IFToMM International Conference on Reconfigurable Mechanisms and Robots, London, UK, 2009, pp. 1–7.
[29] C.C. Lee, J.M. Hervé, Discontinuously movable seven-link mechanisms via group-algebraic approach, Proceedings of the Institution of Mechanical Engineers, Part C: Journal of Mechanical Engineering Science 219 (2005) 577–587.
[30] C.Y. Song, Y. Chen, Multiple linkage forms and bifurcation behaviours of the double-subtractive-Goldberg linkage, Mechanism and Machine Theory 57 (2012) 95–110.
[31] C.Y. Song, Y. Chen, A special Wohlhart's double-Goldberg 6*R* linkage and its multiple operation forms among 4*R* and 6*R* linkages, Advances in Reconfigurable Mechanisms and Robots I, Springer, London, 2012. 45–52.
[32] A.T. Yang, Application of Quaternion Algebra and Dual Numbers to the Analysis of Spatial Mechanisms, Columbia University, 1963.
[33] C. Mavroidis, B. Roth, On the geometry of spatial polygons and screw polygons, Journal of Mechanical Design, Transaction of the ASME 119 (1997) 246–252.
[34] C.T. Huang, C.M. Chen, The linear representation of the screw triangle—a unification of finite and infinitesimal kinematics, Journal of Mechanical Design, Transaction of the ASME 117 (1995) 554–560.
[35] C.T. Huang, The screw triangle: now and then, in: M. McCarthy (Ed.), Bernard Roth Symposium, Stanford, 2003.
[36] J. Denavit, R.S. Hartenberg, A kinematic notation for lower-pair mechanisms based on matrices, Journal of Applied Mechanics, Transactions of the ASME 23 (1955) 215–221.
[37] C. Dalha, Le Mécanisme de Bennett: propriétés et applications, Laboratoire de Mécanique appliquée, Besançon, France, 1982. 151.
[38] J.M. Hervé, M. Dahan, The two kinds of Bennett's mechanisms, Proceedings of the Sixth World Congress on Theory of Machines and Mechanisms, New Delhi, India, 1983, pp. 116–119.
[39] J.E. Baker, An analysis of the Bricard linkages, Mechanism and Machine Theory 15 (1980) 267–286.
[40] C.Y. Song, Kinematic Study of Overconstrained Linkages and Design of Morphing Structures, Nanyang Technological University, 2013. , (PhD thesis).
[41] W.W. Gan, S. Pellegrino, A numerical approach to the kinematic analysis of deployable structures forming a closed loop, Proceedings of the Institution of Mechanical Engineers, Part C: Journal of Mechanical Engineering Science 220 (2006) 1045–1056.
[42] S. Pellegrino, Structural computations with the singular value decomposition of the equilibrium matrix, International Journal of Solids and Structures 30 (1993) 3025–3035.